

Flaring up of the Compact Cloud G2 during the Close Encounter with Sgr A*

Takayuki R. SAITOH¹, Junichiro MAKINO^{1,2}, Yoshiharu ASAKI³, Junichi BABA¹, Shinya KOMUGI⁴, Makoto MIYOSHI⁴, Tohru NAGAO⁵, Masaaki TAKAHASHI⁶, Takaaki TAKEDA^{4,7}, Masato TSUBOI³, & Ken-ichi WAKAMATSU⁸

¹ Earth-Life Science Institute, Tokyo Institute of Technology, 2–12–1, Ookayama, Meguro, Tokyo, 152-8551, Japan

² RIKEN Advanced Institute for Computational Science, 7–1–26, Minatojima-minami-machi, Chuo-ku, Kobe, Hyogo 650-0047, Japan

³ Japan Aerospace Exploration Agency, 3–1–1, Yoshinodai, Chuo-ku, Sagami-hara, Kanagawa 252-5210, Japan

⁴ National Astronomical Observatory of Japan, 2–21–1, Oosawa, Mitaka, Tokyo 182-8588, Japan

⁵ Kyoto University, Kitashirakawa-Oiwake-cho, Sakyo-ku, Kyoto 606-8502, Japan

⁶ Aichi University of Education, 1 Hirosawa, Igaya-cho, Kariya, Aichi 448-8542, Japan

⁷ VASA Entertainment Co., Ltd., 4-14-17, Sennincho, Hachioji, Tokyo, 193-0835, Japan

⁸ Gifu University, 1–1 Yanagido, Gifu City 501-1193, Japan
saitoh@geo.titech.ac.jp

(Received 2013 May 27; accepted 2013 Aug 6)

Abstract

A compact gas cloud G2 is predicted to reach the pericenter of its orbit around the super massive black hole (SMBH) of our galaxy, Sagittarius A* (Sgr A*). This event will give us a rare opportunity to observe the interaction between SMBH and gas around it. We report the result of the fully three-dimensional simulation of the evolution of G2 during the first pericenter passage. The strong tidal force by the SMBH stretches the cloud along its orbit, and compresses it strongly in the vertical direction, resulting in the heating up and flaring up of the cloud. The bolometric luminosity will reach the maximum of $\sim 100 L_{\odot}$. This flare should be easily observed in the near infrared.

Key words: Galaxy:center—Galaxy:nucleus—methods:numerical

1. Introduction

At present, the activity of Sgr A* seems to be in the low-state, with the X-ray luminosity of 10^{33} erg s⁻¹ (Baganoff et al. 2003). There are evidences of past activities (Sunyaev et al. 1993; Koyama et al. 1996; Dobler et al. 2010; Su et al. 2010), where the luminosity had reached as high as $\sim 10^{40}$ erg s⁻¹. Recently, rapid flaring from Sgr A* was observed in various wave lengths (Tsuboi et al. 1999; Baganoff et al. 2001; Genzel et al. 2003; Miyazaki et al. 2004). Thus, it is quite important to understand how these large variations in the luminosity took place. One possibility is the intermittent supply of gas in the form of high-density clouds.

The compact cloud G2 (Gillessen et al. 2012) might be offering us the first opportunity to study such an interaction of a gas cloud and SMBH. While the formation mechanism of the cloud is under debate (Burkert et al. 2012; Gillessen et al. 2012; Miralda-Escudé 2012; Murray-Clay & Loeb 2012; Meyer & Meyer-Hofmeister 2012; Scoville & Burkert 2013), we know that the orbit of G2, determined from observations since 2004, is highly eccentric, and G2 will reach the pericenter of its orbit in the mid 2013 (2013.51 ± 0.04), with the pericenter distance of only 270 au (Gillessen et al. 2012). Gillessen et al. (2013a) reported the updates of pericentric distance and pericenter passage epoch as 190 au and Sep 2013 (2013.69 ± 0.04), respectively. Phifer et al. (2013) reported

different values of 130 au and Mar 2014 (2014.21 ± 0.14). In Gillessen et al. (2013b), these are now 210 au and Mar 2014 (2014.25 ± 0.06).

Schartmann et al. (2012) studied the evolution of G2 using high-resolution adoptive mesh refinement calculation in two dimensions. In their calculation, the cloud loses the kinetic energy during the pericenter passage due to the ram pressure from the hot atmosphere around the SMBH, and gas accretion to SMBH starts in early 2013, and continues for several decades with a nearly constant accretion rate.

However, it is not clear if the two-dimensional calculation is appropriate or not. The cloud should experience strong compression in the direction perpendicular to the orbital plane, due to the tidal force from the SMBH, resulting in a very thin structure. Because of this structure change, the ram pressure might become ineffective unlike two-dimensional simulations. In addition, this compression energy is emitted via radiation immediately. It is therefore expected that the luminosity of the cloud will increase during the pericenter passage. Since the tidal force in the vertical direction is proportional to the distance from the orbital plane, the cloud will contract uniformly. There is no shock during this contraction, as long as the cloud maintains a finite thickness. Anninos et al. (2012) carried out the three-dimensional mesh simulations, but they neglected the effects of the radiative cooling and therefore did not notice this brightening.

In order to study these effects, we performed fully three-dimensional simulations, in which the compressional heating and radiative cooling of the cloud are consistently taken into account.

2. Method

We solved the evolution of a system consisting of Sgr A*, hot-ambient gas, and the cloud by N -body/Smoothed Particle Hydrodynamics (SPH) simulations. Here, we adopted the compact cloud scenario (Burkert et al. 2012).

We modelled Sgr A* as a sink particle (Bate & Burkert 1997) with the mass of $4.31 \times 10^6 M_{\odot}$ (Gillessen et al. 2009). This sink particle can absorb nearby gas particles. The sink radius is 30 au, which is 350 times larger than the real horizon scale of SMBH, 0.085 au, and is 10 times smaller than the pericenter distance. When a gas particle is absorbed by the sink particle, the gas particle is removed and its mass is added to that of the sink particle. We did not consider the emission from the absorbed gas since observations suggest that accretion flow around Sgr A* is expressed by radiatively inefficient accretion flow (RIAF) (Ichimaru 1977; Narayan & Yi 1994).

A diffuse and hot X-ray emitting gas around Sgr A* (Yuan et al. 2003; Xu et al. 2006) was modelled by Yuan's RIAF model (Yuan et al. 2003), following previous studies of G2 (Gillessen et al. 2012; Burkert et al. 2012; Schartmann et al. 2012). The density and temperature profiles are given by

$$\begin{aligned} \rho_{\text{hot}}(r) &= 1.7 \times 10^{-21} f_{\text{hot}} \left(\frac{1.0 \times 10^{16} \text{ cm}}{r} \right) \text{ g cm}^{-3}, (1) \\ T_{\text{hot}}(r) &= 2.1 \times 10^8 \left(\frac{1.0 \times 10^{16} \text{ cm}}{r} \right) \text{ K}, (2) \end{aligned}$$

where r is the distance from Sgr A* and f_{hot} is the scaling parameter of gas density. We changed f_{hot} from 1.0 (Run 1) through 0.1 (Run 2) to 0 (Run 3) in order to investigate the effect of the hot gas to the evolution of G2. The rotation and inhomogeneity of the hot gas at the initial state were neglected, whereas the dynamical evolution was allowed. Although this profile is convectively unstable (Schartmann et al. 2012), we did not try to prevent the growth of convection. In our model, we allowed the radiative cooling of the hot gas, resulting in the accretion rate consistent to the value suggested by the observation. Because of this accretion flow, the growth of the convection was effectively suppressed.

The cloud, G2, was modelled as a spherical gas cloud of three earth mass and a uniform density distribution. The initial radius of the cloud is 125 au and the initial temperature of the gas is 10^4 K. The orbit of the cloud is that of Gillessen et al. (2012) where the pericenter distance is 270 au and the pericenter passage epoch is 2013.5. We adopted A.D. 1995 as the starting epoch of the simulations and solved the evolution of the cloud for 38 years. This cloud was in the hydrostatic equilibrium with the ambient gas in A.D. 1995, $r_{1995} \simeq 5100$ au: the pressure ratio of the cloud to the hot ambient gas was $1.1/f_{\text{hot}}$. If

the cloud is formed at the apocenter, it should have too elongated structure which is inconsistent to the observation (Burkert et al. 2012).

Particle number, mass and spatial resolutions of the cloud, hot ambient, and SMBH are summarized in Table 1.

We used ASURA, a parallel N -body/SPH simulation code, for these simulations (Saitoh et al. 2008; Saitoh et al. 2009). Gravity was solved by the tree with GRAPE method (Makino 1991b). A symmetrized potential was used in order to accelerate the gravity calculation with tree with the individual softening length (Saitoh & Makino 2012). In this study, we adopted the density independent SPH (Saitoh & Makino 2013) in which the pressure, or the energy density, is evaluated first, and other quantities are evaluated using the pressure. This formulation can successfully handle hydrodynamical instabilities. This ability would be important since according to Burkert et al. (2012), the hydrodynamical instabilities might play important roles in the cloud evolution, in particular at the pericenter. We used the second order symplectic integrator, the leap-frog method, and the individual time-step method (McMillan 1986; Makino 1991a). The FAST method (Saitoh & Makino 2010) and the time-step limiter (Saitoh & Makino 2009) were also used.

We adopted the Monaghan type artificial viscosity term (Monaghan 1997) to handle the shock. To avoid the penetration of particles in the vertical direction at the pericenter passage, we adopted a rather large value of the viscosity parameter, $\alpha = 6$. The radiative cooling and the photoelectric heating due to the far-ultraviolet (FUV) field were taken into account in the form of a cooling/heating function (Wada et al. 2009; Wolfire et al. 1995) and an optically thin approximation was used. With this function, the FUV heating is modelled through the heating rate G_0 (see appendix B in Wada et al. 2009). The covered range of G_0 is $0 - 10^4$, which corresponds to $0 - 6,000$ times as that at the solar neighborhood. On the other hand, if we assume that the FUV heating is proportional to the local stellar density, it is 10^7 times as that of the solar neighborhood. The stellar density at the galactic center is $\sim 10^6 M_{\odot} \text{ pc}^{-3}$ (Genzel et al. 1996; Haller et al. 1996) and that at the solar neighborhood is $\sim 0.05 M_{\odot} \text{ pc}^{-3}$ (Creze et al. 1998; Holmberg & Flynn 2000). Therefore, we could not give FUV heating sufficient strength. We will discuss what is expected when we used $G_0 \sim 10^7$ in §4.2. We assumed $2 Z_{\odot}$ for gas, since the metallicity fraction at the galactic central region is $1.5 - 3 Z_{\odot}$ (Genzel et al. 2010).

Since the radiative cooling is very strong, the temperature of the gas cloud is always less than 10^4 K. This is the reason why previous studies excluded the radiative cooling and often assumed adiabatic or isothermal EOS (Burkert et al. 2012; Schartmann et al. 2012; Anninos et al. 2012). However, as we show in this paper, to include the effect of the radiative cooling is quite important to predict the evolution of luminosity.

Table 1. Number of particles and mass and spatial resolutions

Component	Number	Particle mass	Softening length
Cloud (Run 1)	1×10^6	$3 \times 10^{-6} M_{\oplus}$	0.43 au
Cloud (Run 2)	3×10^5	$1 \times 10^{-5} M_{\oplus}$	0.65 au
Cloud (Run 3)	10^7	$3 \times 10^{-7} M_{\oplus}$	0.20 au
Hot gas (Run 1)	1×10^7	$2.8 \times 10^{-5} M_{\oplus}$	0.92 au
Hot gas (Run 2)	3×10^6	$9.4 \times 10^{-5} M_{\oplus}$	0.63 au
Hot gas (Run 3)	N/A	N/A	N/A
SMBH (Run 1,2,3)	1	$4.31 \times 10^6 M_{\odot}$	10 au

3. Results

Figure 1 shows the evolution of the three-dimensional structure of the cloud from A.D. 2006.26 to A.D. 2013.46. For this model, we used $f_{\text{hot}} = 1$ which is similar to that used in the previous two-dimensional calculation (Burkert et al. 2012; Schartmann et al. 2012). At A.D. 2006, the simulated G2 was nearly spherical, since the effect of the tidal force is inefficient. The destruction effect due to hydrodynamical instabilities is also inefficient since the time scale of instabilities is sufficiently long, ~ 10 yr (Gillessen et al. 2012). By A.D. 2012.02, it is stretched in the orbital plane and compressed in the vertical direction. This stretch has already been observed (Gillessen et al. 2012). When the cloud passes the pericenter, its thickness reaches the minimum. Due to this strong vertical compression, the gas density increases by more than two orders of magnitude.

In the last panels (panels d and d'), we can see the "bridge" between the central SMBH and the head of the cloud. This bridge indicates that there is a flow of gas from the head of the cloud to the SMBH. However, the amount of the gas in this bridge, and the resulting accretion rate to SMBH, are small.

Figure 2 shows the history of accretion rates. We show the results from two runs out of the three runs. For the first run, we used the cloud model the same as that used in Burkert et al. (2012) and Schartmann et al. (2012), except that we solve the dynamical evolution of the hot ambient. Whether or not such high-density, high-temperature atmosphere actually exists near SMBH is an open question. In order to test the importance of the assumption on the hot atmosphere, we performed two additional simulations. In the second run, we reduced the gas density by a factor of 10 (red dashed curve in the figure), and in the third run we eliminated the atmosphere altogether.

In the case of the standard run, the accretion rate of the gas from the cloud reaches the peak value of $\sim 10^{-7} M_{\odot} \text{ year}^{-1}$ at A.D. 2014, and then decreases exponentially. The accretion rate at A.D. 2030 is one order of magnitude smaller than the peak value.

These behaviours are quite different from those in two-dimensional calculations (Schartmann et al. 2012), in which the accretion rate is nearly constant due to the strong ram pressure. In our three-dimensional simulations, the height of the cloud is reduced to 1/100 of the initial value at the pericenter, resulting in the decrease

of the effect of the ram pressure by a similar factor (see §4.1). The total amount of the mass accretion from the gas cloud till A.D. 2023.5, the first ten years from the pericenter passage, is 15% of the cloud mass for Run 1. This accretion rate of Run 1 is comparable to that obtained in a two-dimensional simulation (Schartmann et al. 2012). Since the gas cloud in our three-dimensional simulation is vertically compressed, one might expect a much lower accretion rate. The main reason for this high accretion rate is that in our model the "ambient" gas is accreted to the SMBH, carrying the gas removed from the cloud. In the two-dimensional simulation of Schartmann et al. (2012), the ambient gas is pinned to the original position. Note that the higher accretion rate of the hot ambient gas indicates that, even if we assumed a relatively high density for the halo gas, it is probably difficult to observe the change of the activity of Sgr A* due to this additional accretion.

The overall evolution of the accretion rate depends strongly on the assumed density of the hot atmosphere. When we reduced the hot gas density by a factor of 10, the accretion rate decreased by the same factor. The total amount of the accreted mass during the first ten years from the pericenter passage is $\sim 2\%$ of the original cloud mass. In the run with no halo gas, no gas is accreted to the SMBH.

Figure 3 shows the evolution of the bolometric luminosity of the cloud, for three different models. We integrated the cooling rate of the gas particles during simulations. Note that we neglect the emission from the gas absorbed by Sgr A*, because the accretion around Sgr A* is expected as RIAF. In all of three runs the luminosity peaks at the time of the pericenter passage. Before the pericenter passage, the luminosity is almost constant for the standard run, but goes down for other two runs. In the case of the standard run, there is friction with the hot gas supplies the thermal energy to the cloud, and the luminosity is kept nearly constant. For other two runs, the hot gas is much less dense and heating effect is much smaller. However, the model variation would vanish when we assume much stronger heating rate which is adequate to reproduce the environment of the galactic center region (see §4.2). The peak luminosity and its duration is practically independent of the assumption for the hot atmosphere. This result is quite natural, since the peak luminosity comes mainly from the tidal compressional heating of the cloud and has nothing to do with the interaction with the atmosphere. On the other hand, the interaction with hot

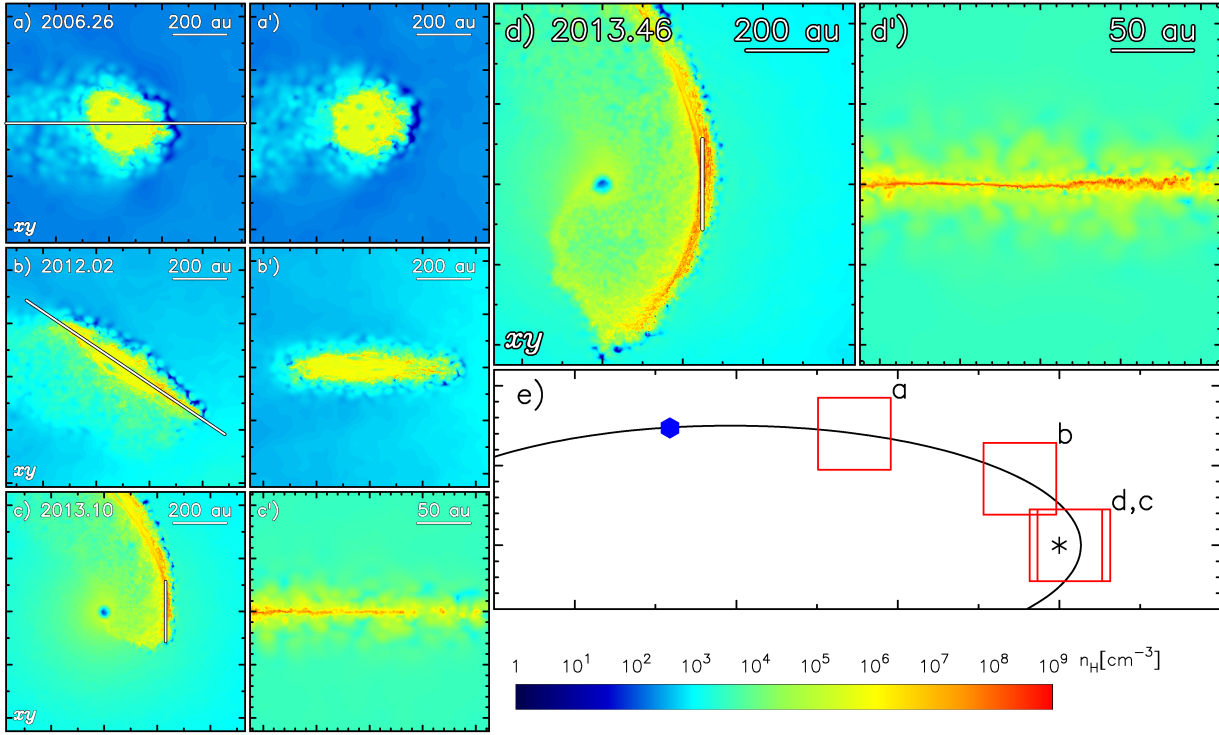


Fig. 1. Time evolution of the structure of G2 for the period of A.D. 2006.26 to A.D. 2013.46, tagged with a to d and a' to d'. The density distributions in the xy planes (a to d) and the selected planes (a' to d') are shown. Here, the xy plane is corresponding to the orbital plane of G2. The thin solid lines in the panels for xy planes show the location of the plane for which the density distributions are shown in the panels in the corresponding panels for selected planes. The top-right two panels shows the distribution at A.D. 2013.46. The left two columns show the view in xy and selected planes, respectively. The panel e depicts part of the orbit of G2 (solid curve) and the positions of the xy planes in the four epochs (red squares). The blue hexagon indicates the position of the cloud at A.D. 1995.5. The plotted region is $-7000 \text{ au} < x < 2000 \text{ au}$ and $-800 \text{ au} < y < 2200 \text{ au}$.

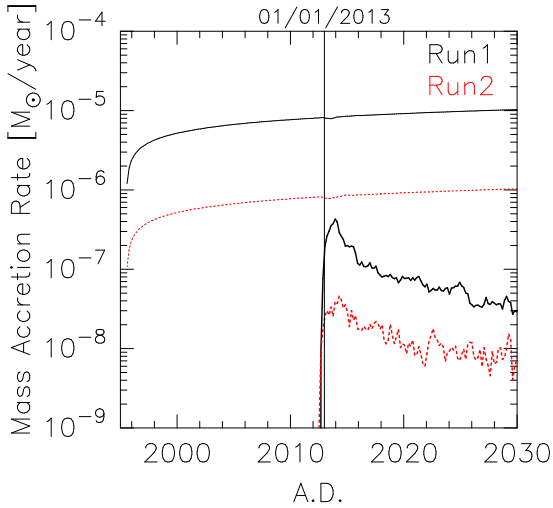


Fig. 2. Time evolution of the accretion rate of the gas to the SMBH. Black and red curves are the results of simulations with the standard high-density hot atmosphere (Run1) and with low-density atmosphere (Run2), respectively. Thick curves show accretion rates of the cloud gas, and thin curves show those of the halo gas. The vertical line denotes the epoch of 01/01/2013. When we excluded the hot ambient, there was no accretion to the SMBH.

atmosphere keeps the luminosity high for years before and after the pericenter passage. We will give rough estimate of the effect of ram-pressure heating in §4.1.

We can estimate the total amount of the energy generated by the tidal compressional heating in the following way. For simplicity, let's assume that gas moves freely until it reaches the equatorial plane, where it converts all the kinematic energy of its vertical motion to thermal energy. This is of course not a realistic assumption, since the gas is heated due to the compression and emits radiation. Therefore, strictly speaking, what is given below is the upper bound. The vertical velocity is given by $V_v = V_a \tan i$, where V_a is the velocity at the ascending node and i is the inclination. If we assume that the cloud was still spherical around year A.D. 2000 where the cloud was around the one of vertice, we have

$$V_v \simeq 440 \left(\frac{V_a}{5300 \text{ km}^{-1}} \right) \left(\frac{R_c}{125 \text{ au}} \right) \left(\frac{1500 \text{ au}}{R_b} \right) \text{ km s}^{-1} \quad (3)$$

for a gas element 125 au from the orbital plane at A.D. 2000. Here, R_c is the radius of the cloud when the cloud is on the minor axis of its orbit and R_b is the distance to the vertice in the semi-minor axis. By integrating the energy over the spherical cloud of radius R_c , we have

$$\frac{dE_t}{dt} \simeq 2.2 \times 10^{35} \left(\frac{V_a}{5300 \text{ km}^{-1}} \right)^2 \left(\frac{1500 \text{ au}}{R_b} \right)^2$$

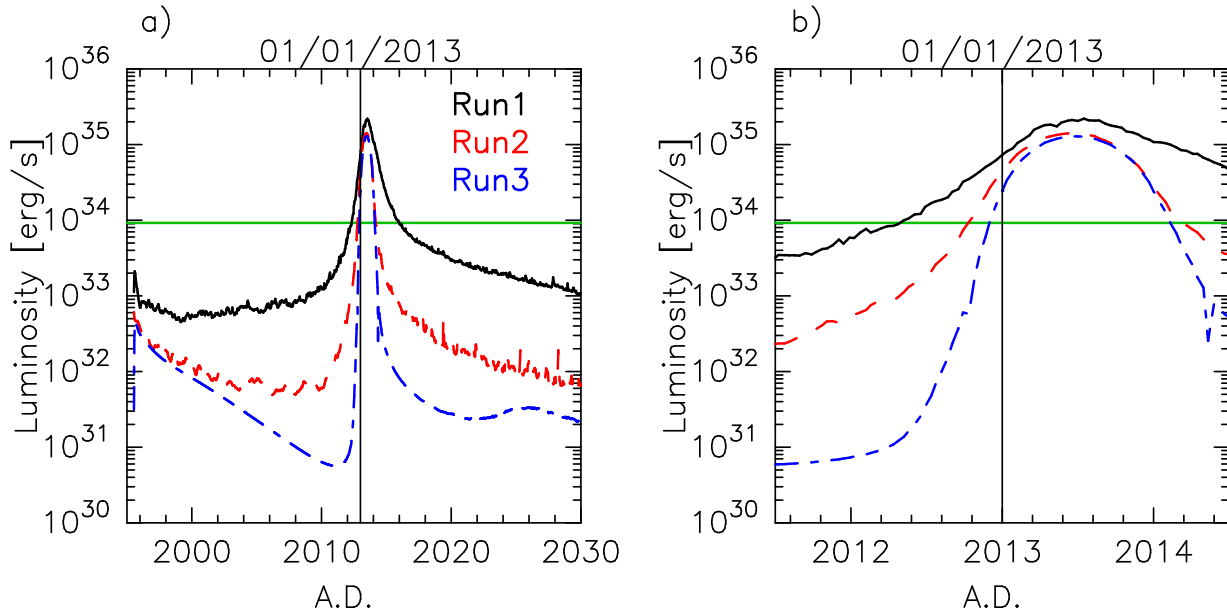


Fig. 3. Bolometric luminosity as a function of time. Panel a shows the time evolution of the luminosity from A.D. 1995 to A.D. 2030, while panel b shows it from A.D. 2011.5 to 2014.5. Solid black, red dashed and blue dot-dashed curves are the results from simulations with the standard high-density atmosphere (Run1), with low-density atmosphere (Run2), and no atmosphere (Run3), respectively. The green horizontal line indicates the expected luminosity of 9.2×10^{33} erg s $^{-1}$ under the strong heating rate with $G_0 = 1.7 \times 10^7$. See the text in §4.2.

$$\left(\frac{M_c}{3M_\oplus}\right) \left(\frac{R_c}{125 \text{ au}}\right)^2 \left(\frac{1 \text{ year}}{\tau}\right) \text{ erg s}^{-1}, \quad (4)$$

where M_c is the cloud mass. We assume that vertical velocity is zero at that moment. In other words, we assume that the ascending node coincides with the pericenter. The duration time of energy release τ is about one year, as we can see from figure 3.

The radiative energy loss rate of the cloud is given by

$$\frac{dE_{\text{cooling}}}{dt} \simeq 1.1 \times 10^{39} \left(\frac{n_H}{10^5 \text{ cm}^{-3}}\right) \left(\frac{M_c}{3M_\oplus}\right) \text{ erg s}^{-1}. \quad (5)$$

Here, we used the cooling coefficient of $\Lambda \sim 10^{-22}$ erg cm 3 s $^{-1}$ at the gas of 10^4 K (Sutherland & Dopita 1993). Since the cooling rate is sufficiently large, it is possible to keep the temperature of the cloud to $\sim 10^4$ K (see also figure 4), and therefore the emission is mostly in hydrogen recombination lines.

This simple estimate is in good agreement with the total amount of radiation in our detailed simulations, although the actual evolution process would be much complex. Note that the total amount of radiation depends on the height and vertical velocity structure of the cloud. For example, if the compression velocity is zero at the apocenter, the inclination would be smaller by a factor of a few, resulting in the decrease of the total luminosity by about one order of magnitude.

Figure 4 shows the distributions of temperature and brightness, for selected moments. Here, only the gas component which is initially associated with the gas cloud is considered in this figure. The main body of the gas cloud is heated up by the compression, but the temperature remains near 10^4 K due to very efficient radiative cooling of

ionized hydrogen through recombination lines. The most luminous region is several hundred aUs in size. They are most likely to be observable from the outside in the near infrared, which does not suffer from the dust extinction effects significantly.

4. Discussion & Summary

4.1. Contribution of Ram Pressure in Three-dimensional Simulations

The ram pressure of the hot ambient to the cloud is evaluated as

$$P(r) = \rho_{\text{hot}}(r)v_c(r)^2, \quad (6)$$

where ρ_{hot} is the density of the hot ambient gas and v_c is the velocity of the cloud relative to the hot ambient. When we assume that some part of the work of the pressure force is converted to the thermal energy of the cloud, the heating rate is

$$\frac{dE_{\text{ram}}}{dt} = C\sigma P(r)v_c(r) = C\sigma\rho_{\text{hot}}(r)v_c(r)^3, \quad (7)$$

where σ is the cross-section of the cloud, *i.e.*, the size of the cloud projected to the plane perpendicular to its motion, and C is the conversion efficiency. By using the density profile of the hot ambient gas (Eq. 1) and the relation between r and v_c (see Eq. 1 in Burkert et al. 2012), we have

$$\frac{dE_{\text{ram}}}{dt} \simeq 8.2 \times 10^{33} C f_{\text{hot}} \left[\frac{\sigma}{\pi(125 \text{ au})^2} \right] \left(\frac{6 \times 10^{16} \text{ cm}}{r} \right) \left[\left(\frac{6 \times 10^{16} \text{ cm}}{r} \right) - 0.46 \right]^{3/2} \text{ erg s}^{-1}. \quad (8)$$

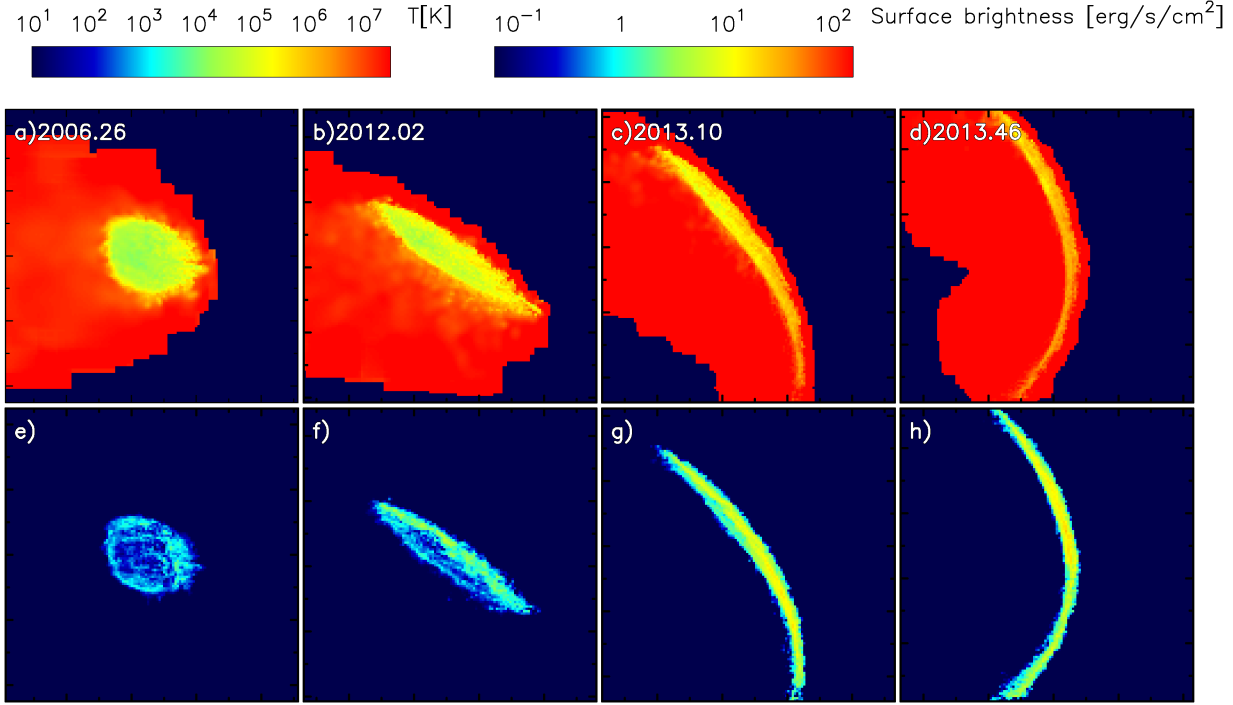


Fig. 4. Time evolution of the gas temperature and integrated surface luminosity from gas with a temperature range of 8000 – 15000 K from A.D. 2006.26 to A.D. 2013.46, tagged with a to d and e to h. The face-on view (the xy plane) is assumed and each panel shows a 900 au \times 900 au region.

We can see that the heating rate depends both on the distance from the SMBH and the cross section of the cloud, *i.e.*, r and σ . Thus, to estimate the time variation of the heating due to the ram pressure, we need to estimate the time variation of the cross-section.

As an example, we evaluate the ram-pressure heating rate at the pericenter. From figure 1, the cross-section of the cloud at the pericentre is $\sigma_{\text{A.D.2013.5}} \sim 1 \text{ au} \times 40 \text{ au} = 40 \text{ au}^2$. The thickness of 1 au is affected by the resolution limit, and in reality the cloud is probably even more thinner. Hence, the estimate below gives the upper limit. Substituting this value and $r = r_{\text{A.D.2013.5}} = 4 \times 10^{15} \text{ cm}$ into Eq. 8, we have

$$\left(\frac{dE_{\text{ram}}}{dt} \right)_{\text{A.D.2013.5}} \leq 5.6 \times 10^{33} C f_{\text{hot}} \text{ erg s}^{-1}. \quad (9)$$

Even when we adopt $C = 1$, this value is nearly two orders of magnitude smaller than that by the tidal heating (see Eq. 4). The ram pressure is not the primary source of the luminosity of the cloud.

As the other example, we evaluate Eq. 8 at A.D. 2000, where $r_{\text{A.D.2000}} = 6 \times 10^{16} \text{ cm}$. We assume that the cloud shape maintains the original spherical shape at this moment. Therefore, $\sigma_{\text{A.D.2000}} \sim \pi(125 \text{ au})^2$. By substituting these values, we obtain

$$\left(\frac{dE_{\text{ram}}}{dt} \right)_{\text{A.D.2000}} \simeq 3.3 \times 10^{33} C f_{\text{hot}} \text{ erg s}^{-1}. \quad (10)$$

This rate is about three times higher than the result of our simulation. If we assume $C \sim 0.3$, the ram-pressure

heating explains the luminosity before pericenter passage in our simulation fairly well.

4.2. Cloud Luminosity before the Pericenter Passage

As described in §2 and §3, the adopted heating rate due to FUV in our simulations was too low compared to the expected value. Here, we discuss the expected bolometric luminosity before the pericenter passage.

According to Bakes & Tielens (1994), the heating rate due to the photoelectric heating by the far-ultraviolet field is

$$n_{\text{H}} \Gamma = 10^{-24} n_{\text{H}} G_0 \epsilon_0 \text{ erg cm}^{-3} \text{ s}^{-1}, \quad (11)$$

where G_0 is the coefficient of the heating rate and ϵ_0 is the efficiency and we deal with this as a constant value 0.05, although it depends weakly on G_0 , T , and n_{H} (Bakes & Tielens 1994). The heating rate of the cloud is, thus,

$$\frac{dE_{\text{heating}}}{dt} \simeq 5.4 \times 10^{28} \left(\frac{M_{\text{c}}}{3M_{\oplus}} \right) \left(\frac{G_0}{10^2} \right) \left(\frac{\epsilon_0}{0.05} \right) \text{ erg s}^{-1}. \quad (12)$$

As discussed in §2, we could not use $G_0 > 10^4$, and the actual value we used is 10^2 . This value is quite low and hence we cannot observe the effect of the heating in figure 3.

The expected value of G_0 is $\sim 1.7 \times 10^7$, which gives the heating rate of $9.2 \times 10^{33} \text{ erg s}^{-1}$. The green horizontal line in figure 3 indicates this luminosity. In this case, the heating rate is always larger than the heating by the ram pressure. Thus, FUV heating should be the primary source of the cloud luminosity before the pericenter passage and all runs show the same and constant luminosity.

The time independent luminosity is consistent with the observations (See also §4.3).

4.3. Luminosity in the Br γ line

Based on our simulation results, we discuss the Br γ magnification during the pericenter passage. Since the main cooling mechanism of the gas cloud is the line cooling, we computed the fraction of the Br γ line luminosity to the total emission-line luminosity, F . For this computation, we used the publicly available code Cloudy ver. c10.00 (Ferland et al. 1998). We assumed a compressed gas with the hydrogen density of 10^{6-8} cm $^{-3}$, the solar chemical abundances, and typical grains. We then computed the emission-line spectrum when this gas is heated to be 2×10^4 K. We found that $F \sim 0.1\%$.

By multiplying F to the bolometric luminosity, we have the Br γ luminosity of several $\times 10^{32}$ erg s $^{-1}$ at A.D. 2013.5. According to Gillessen et al. (2012) and Gillessen et al. (2013a), the intrinsic luminosity of the Br γ line from G2 is 0.166% – 0.2% of the solar luminosity, $\sim 7 \times 10^{30}$ erg s $^{-1}$ during A.D. 2004–2012. Thus, the Br γ luminosity at the peak will reach to nearly 100 times that of observed values before the pericenter passage.

Applying the value of F to the expected luminosity before the pericenter passage we obtained in §4.2, we obtain the constant Br γ flux of $\sim 10^{-3}L_{\odot}$. This value is consistent with the observational results that the Br γ flux is $\sim 2 \times 10^{-3}L_{\odot}$ and almost constant during this nine years since A.D. 2004 (Gillessen et al. 2012; Gillessen et al. 2013a; Gillessen et al. 2013b).

4.4. Peak Bolometric Luminosities with Different Orbits

So far, four studies have reported the orbital information of G2 and there are some variations. Here, we evaluate the peak luminosities of the cloud due to the tidal compression in these orbits.

Table 2 summarizes the orbital information of four studies (Gillessen et al. 2012; Gillessen et al. 2013a; Gillessen et al. 2013b; Phifer et al. 2013) and expected peak luminosities evaluated by Eq. 4. Note that we assumed the same duration time for all orbits. From this table, we can see that the variations of the expected peak luminosities are at most a factor of three. The orbit reported by Phifer et al. (2013) gives the highest luminosity, reflecting the highest eccentricity and the closest pericentric distance.

We also note that the time for which the cloud will stay around the pericenter decreases when the V_a increases. As a result, the rise and decay of the light curve become steeper and the duration time decreases. This should change the peak luminosity of the light curve, but we do not take this point into account in this table. Simulations with different orbits are necessary to have concrete expectations and we will show them in the near future.

4.5. Summary

We have performed fully three-dimensional simulations of the evolution of the G2 cloud. Our result differs from the result of previous two-dimensional simulations in (i) strong vertical compression leads to the heating up and

flaring up of the cloud at the first pericenter passage, and (ii) because of this compression, ram-pressure drag from the hot atmosphere is ineffective in removing the energy and angular momentum of the cloud.

In our standard model, the peak luminosity would reach ~ 100 times the solar luminosity. The luminosity depends on the assumed internal velocity structure of the cloud, and thus might be fainter by one order of magnitude. Since the peak luminosity is from the tidal compressional heating, it does not depend on the assumption on the structure of the hot atmosphere around the SMBH. We therefore believe that our prediction is pretty robust.

The increase of the luminosity of the cloud would be detectable in near infrared bands about six months before the pericenter passage epoch. In parallel, the increase of the vertical velocity is probably observable as the line broadening. Since the vertical velocity should strongly depend on the position of the gas on the orbit, it is very important to measure the variation of the velocity profile both in space and time.

Detailed comparison between high-accuracy three-dimensional calculations and observation will help us to understand the nature of the cloud and how it will interact with the SMBH.

We thank the anonymous referee for his/her insightful comments and suggestions, which helped us to greatly improve our manuscript. Numerical simulations were carried out on the Cray XT4 and XC30 systems in CfCA at NAOJ. This work is supported by SPIRE.

References

- Anninos, P., Fragile, P. C., Wilson, J., & Murray, S. D. 2012, *ApJ*, 759, 132
- Baganoff, F. K., et al. 2001, *Nature*, 413, 45
- , 2003, *ApJ*, 591, 891
- Bakes, E. L. O., & Tielens, A. G. G. M. 1994, *ApJ*, 427, 822
- Bate, M. R., & Burkert, A. 1997, *MNRAS*, 288, 1060
- Burkert, A., Schartmann, M., Alig, C., Gillessen, S., Genzel, R., Fritz, T. K., & Eisenhauer, F. 2012, *ApJ*, 750, 58
- Creze, M., Chereul, E., Bienayme, O., & Pichon, C. 1998, *A&A*, 329, 920
- Dobler, G., Finkbeiner, D. P., Cholis, I., Slatyer, T., & Weiner, N. 2010, *ApJ*, 717, 825
- Ferland, G. J., Korista, K. T., Verner, D. A., Ferguson, J. W., Kingdon, J. B., & Verner, E. M. 1998, *PASP*, 110, 761
- Genzel, R., Eisenhauer, F., & Gillessen, S. 2010, *Reviews of Modern Physics*, 82, 3121
- Genzel, R., Schödel, R., Ott, T., Eckart, A., Alexander, T., Lacombe, F., Rouan, D., & Aschenbach, B. 2003, *Nature*, 425, 934
- Genzel, R., Thatte, N., Krabbe, A., Kroker, H., & Tacconi-Garman, L. E. 1996, *ApJ*, 472, 153
- Gillessen, S., Eisenhauer, F., Trippe, S., Alexander, T., Genzel, R., Martins, F., & Ott, T. 2009, *ApJ*, 692, 1075
- Gillessen, S., et al. 2012, *Nature*, 481, 51
- , 2013a, *ApJ*, 763, 78
- , 2013b, *ArXiv e-prints:1306.1374*
- Haller, J. W., Rieke, M. J., Rieke, G. H., Tamblyn, P., Close, L., & Melia, F. 1996, *ApJ*, 456, 194

Table 2. Orbital Information and Expected Peak Luminosities

	Gillessen et al. (2012)	Gillessen et al. (2013a)	Gillessen et al. (2013b)	Phifer et al. (2013)
r_{peri}^*	270 au	190 au	210 au	130 au
e^\dagger	0.938	0.966	0.976	0.981
R_a^\ddagger	4300 au	5240 au	8750 au	6840 au
R_b^\S	1490 au	1350 au	1910 au	1330 au
V_a^\parallel	5300 km s ⁻¹	6480 km s ⁻¹	6010 km s ⁻¹	7610 km s ⁻¹
$V_t^\#$	450 km s ⁻¹	600 km s ⁻¹	390 km s ⁻¹	710 km s ⁻¹
$\frac{dE_t}{dt}^{**}$	2.2×10^{35} erg s ⁻¹	4.1×10^{35} erg s ⁻¹	1.8×10^{35} erg s ⁻¹	5.8×10^{35} erg s ⁻¹

* Pericentric distance.

† Eccentricity.

‡ Length of semi-major axis.

§ Length of semi-minor axis.

∥ V_a is evaluated with the Sgr A* mass of $4.31 \times 10^6 M_\odot$ (Gillessen et al. 2009).

Eq. 3 is used.

** Eq. 4 is used. The duration time is fixed as one year.

Holmberg, J., & Flynn, C. 2000, MNRAS, 313, 209

Ichimaru, S. 1977, ApJ, 214, 840

Koyama, K., Maeda, Y., Sonobe, T., Takeshima, T., Tanaka, Y., & Yamauchi, S. 1996, PASJ, 48, 249

Makino, J. 1991a, PASJ, 43, 859

—. 1991b, PASJ, 43, 621

McMillan, S. L. W. 1986, in Lecture Notes in Physics, Berlin Springer Verlag, Vol. 267, The Use of Supercomputers in Stellar Dynamics, ed. P. Hut & S. L. W. McMillan, 156–+

Meyer, F., & Meyer-Hofmeister, E. 2012, A&A, 546, L2

Miralda-Escudé, J. 2012, ApJ, 756, 86

Miyazaki, A., Tsutsumi, T., & Tsuboi, M. 2004, ApJL, 611, L97

Monaghan, J. J. 1997, Journal of Computational Physics, 136, 298

Murray-Clay, R. A., & Loeb, A. 2012, Nature Communications, 3

Narayan, R., & Yi, I. 1994, ApJL, 428, L13

Phifer, K., et al. 2013, ArXiv e-prints:1304.5280

Saitoh, T. R., Daisaka, H., Kokubo, E., Makino, J., Okamoto, T., Tomisaka, K., Wada, K., & Yoshida, N. 2008, PASJ, 60, 667

—. 2009, PASJ, 61, 481

Saitoh, T. R., & Makino, J. 2009, ApJL, 697, L99

—. 2010, PASJ, 62, 301

—. 2012, New Astronomy., 17, 76

—. 2013, ApJ, 768, 44

Schartmann, M., Burkert, A., Alig, C., Gillessen, S., Genzel, R., Eisenhauer, F., & Fritz, T. K. 2012, ApJ, 755, 155

Scoville, N., & Burkert, A. 2013, ApJ, 768, 108

Su, M., Slatyer, T. R., & Finkbeiner, D. P. 2010, ApJ, 724, 1044

Sunyaev, R. A., Markevitch, M., & Pavlinsky, M. 1993, ApJ, 407, 606

Sutherland, R. S., & Dopita, M. A. 1993, ApJS, 88, 253

Tsuboi, M., Miyazaki, A., & Tsutsumi, T. 1999, in Astronomical Society of the Pacific Conference Series, Vol. 186, The Central Parsecs of the Galaxy, ed. H. Falcke, A. Cotera, W. J. Duschl, F. Melia, & M. J. Rieke, 105

Wada, K., Papadopoulos, P. P., & Spaans, M. 2009, ApJ, 702, 63

Wolfire, M. G., Hollenbach, D., McKee, C. F., Tielens, A. G. G. M., & Bakes, E. L. O. 1995, ApJ, 443, 152

Xu, Y.-D., Narayan, R., Quataert, E., Yuan, F., & Baganoff, F. K. 2006, ApJ, 640, 319

Yuan, F., Quataert, E., & Narayan, R. 2003, ApJ, 598, 301